Effects of energetic electrons on magnetized electrostatic plasma sheaths

D. Tskhakaya[a] and S. Kuhn
Association Euratom—ÖAW, Department of Theoretical Physics, University of Innsbruck, A-6020 Innsbruck, Austria

V. Petržilka
Institute of Plasma Physics, Academy of Sciences of the Czech Republic, CZ-18221 Prague, Czech Republic

R. Khanal[b]
Association Euratom—ÖAW, Department of Theoretical Physics, University of Innsbruck, A-6020 Innsbruck, Austria

(Received 28 December 2001; accepted 8 March 2002)

The influence of energetic electrons on magnetized plasma sheaths is studied for different current regimes and different secondary-electron emission coefficients. (Here, the term ''plasma sheath'' denotes the collisionless region consisting of the non-neutral Debye sheath and the quasi-neutral magnetic presheath.) It is shown that the presence of even a small population of energetic electrons can significantly influence the potential drop across the sheath and the energy flux to the wall. For example, for plasma parameters typical of contemporary tokamaks, the presence of a fast-electron population with density smaller than 0.1% (!) can double the potential drop across the sheath and the energy flux to the wall, and the presence of a few percent of fast electrons can enhance these values by up to one order. The effect of fast electrons decreases with increasing secondary-electron emission coefficient and increasing current to the wall. Analytical results obtained are checked against particle-in-cell (PIC) simulations for different current regimes and different secondary-electron emission coefficients, showing good agreement except in some cases where the simulation results exhibit strong fluctuations. © *2002 American Institute of Physics.*
[DOI: 10.1063/1.1475310]

I. INTRODUCTION

In the presence of a strong magnetic field, the transition region between a conducting wall and some bulk plasma (''plasma–wall transition, PWT'') consists of the non-neutral Debye sheath (adjacent to the wall), the quasi-neutral magnetic presheath, and the quasi-neutral collisional presheath, extending up to the bulk plasma.[1] In this paper, the region consisting of the Debye sheath and the magnetic presheath will be referred to as the ''plasma sheath,'' so that the ''plasma–sheath edge'' coincides with the magnetic-presheath edge. This region is practically collisionless and characterized by steep gradients of the plasma parameters. The negative potential drop established across the plasma sheath towards the wall acts as a thermal insulator between the (hot) plasma electrons and the wall. Conversely, it accelerates ions before they hit the wall and thus affects, among other things, the impurity sputtering rate. Hence, the plasma sheath (and, in particular, the potential drop across it) can significantly influence the overall operation of a fusion plasma device.

There exists a very large number of papers with analytical, experimental and numerical investigations of plasma sheaths both unmagnetized and magnetized (e.g., Refs. 1–5). In these ''classical'' papers, as in the vast majority of papers on sheaths in general, the electrons were taken to be Boltzmann-distributed, an assumption which can be far from reality. In a real device, the plasma at the sheath edge may contain different electron populations with different temperatures and average velocities, and accordingly the plasma sheath can substantially differ from the ''classical'' one. Similar problems also arise in Langmuir-probe theory as shown in Ref. 6.

The effect of energetic electrons on the *unmagnetized* plasma sheath (which in our terminology is identical with the Debye sheath) and the collisional presheath was analytically and experimentally investigated in various papers, where plasmas with two-temperature electrons (Refs. 6–12) or with an additional high-energy electron beam (Refs. 13–20) were considered. It was shown that the presence of even a very small population of high-energy electrons can significantly change the plasma sheath and presheath characteristics.

In the presence of a tilted magnetic field, the plasma-wall transition becomes very complicated even in the absence of an energetic electron population (e.g., Ref. 21) and requires an analysis substantially different from that applied to the unmagnetized plasma. Fortunately, however, some key sheath parameters of interest to us, such as the total potential drop across the sheath and the particle energy flux to the wall, can be obtained from the plasma parameters at the sheath entrance, without calculating their profiles inside the sheath.[3]

[a]Permanent address: Institute of Physics, Georgian Academy of Sciences, 380077 Tbilisi, Georgia; electronic mail: david.tskhakaya@uibk.ac.at
[b]Permanent address: Department of Physics, Mahendra Morang College, Biratnagar-16, Nepal.

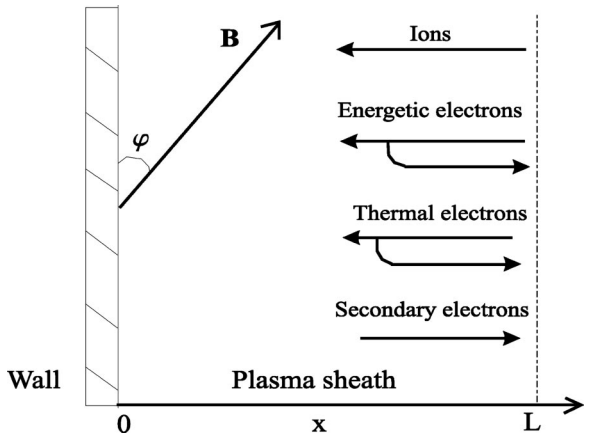

FIG. 1. Plasma sheath. The x axis is normal to the wall surface.

In our previous work (see Ref. 22), we considered a magnetized plasma sheath with two electron components: a low-temperature (majority) and a high-temperature (minority) one, the latter in addition having a sufficiently large fluid (i.e., average) velocity. Our analytical calculations and numerical simulations showed that the presence of even a very small population ($<1\%$) of energetic electrons can significantly increase the potential drop across the sheath and the energy deposition at the target plate (wall). In the present work, we generalize our previous results by including effects of secondary electrons and nonvanishing net current.

Plasma sheaths with an energetic electron population having a large fluid velocity can be formed, e.g., in tokamaks during lower-hybrid (LH) heating and noninductive current drive (CD) experiments. The appearance of these very energetic electrons, which can propagate to the divertor plate and significantly change the plasma parameters there (Refs. 23–26), is a secondary effect of LH operation.

In this paper we present both analytical calculations and 1d3v particle-in-cell (PIC) simulation results, which are found to be in good agreement with each other except in some cases where the simulation results exhibit large fluctuations. For the plasma density and temperature, the magnetostatic field and other parameters entering the simulations, we have chosen values relevant to LHCD experiments performed recently at the Tore Supra tokamak.[27]

II. THEORY

A. Model and basic relations

We consider a collisionless, one-dimensional, stationary, magnetized electrostatic plasma sheath; cf. Fig. 1. The angle between the wall surface and the constant uniform magnetic field is φ; velocity components parallel and perpendicular to the magnetic field will be denoted by the subscripts "$\|$" and "$\perp$," respectively.

The x axis is normal to the conducting wall, with $x=0$ at the wall surface and $x=L$ at the sheath entrance. As usual, the potential is assumed to decrease monotonically towards the wall, which implies that $\varphi > \sqrt{m_e/m_i}$.[28] The potential drop across the sheath is

$$\Delta\Phi \equiv \Phi(0) - \Phi(L) < 0.$$

We consider a model in which there are three electron populations: slow (thermal; majority), fast (energetic) and secondary. We assume that all particles reaching the wall are absorbed, and that at the sheath entrance the average velocities of the slow and fast electrons are directed along the magnetic field. The ions move towards the wall, whereas the electrons, due to reflection by the negative potential drop across the sheath and due to secondary emission from the wall, can move in both directions (Fig. 1). At the sheath entrance, the plasma is quasi-neutral:

$$n_{\rm sl}^0 + n_f^0 + n_s^0 = n_i^0 \equiv n^0, \tag{1}$$

and there exists a constant net electric current density J in the direction normal to the wall. Here and below the subscripts i, sl, f and s denote the ions and the slow, fast and secondary electrons, respectively. In addition we assume the magnetic field to be sufficiently strong, so that the electron gyroradius (ρ_e) is smaller than the Debye length ($\lambda_{\rm D}$) $\rho_e \ll \lambda_{\rm D}$.

From particle conservation, it follows that

$$\partial_x F_{lx} = 0 \quad (l = i, e),$$

i.e., that the normal components of the electron flux ($F_{ex} = F_{{\rm sl}x} + F_{\rm fx} + F_{\rm sx}$) and the ion flux ($F_{ix}$) are constant. They obviously satisfy the equation

$$F_{ex} = F_{ix} - J/e. \tag{2}$$

At the sheath entrance we try to specify as few parameters as possible, assuming that the slow (majority-population) electrons have a cut-off Maxwellian-distribution, and that the fast-electron population is a sum of two cut-off shifted Maxwellian distributions representing the incoming and the reflected fast-particle beams:

$$f_{\rm sl}^0(v_\|, v_\perp) = 2n_{\rm sl}^0 \frac{\exp[-(v_\|^2 + v_\perp^2)/v_{{\rm sl}T}^2] H(v_c - v_\|)}{v_{{\rm sl}T}^3 \pi^{3/2}[1 + \mathrm{erf}(v_c/v_{{\rm sl}T})]},$$

$$f_f^0(v_\|, v_\perp) = \frac{2n_f^0}{v_{fT}^3 \pi^{3/2}[1 + 2\,\mathrm{erf}(v_{f\|}/v_{fT}) + \mathrm{erf}((v_c - v_{f\|})/v_{fT})]} \times \{\exp[-((v_\| + v_{f\|})^2 + v_\perp^2)/v_{fT}^2] H(-v_\|) + \exp[-((v_\| - v_{f\|})^2 + v_\perp^2)/v_{fT}^2] H(v_\|) H(v_c - v_\|)\}, \tag{3}$$

where $v_{sT} = \sqrt{2T_s/m_e}$ $(s = {\rm sl}, f)$ is the species-s thermal velocity, $-v_{f\|}$ and $v_{f\|}$ are the "shift velocities" of the primary and reflected fast electrons, respectively, $v_c = \sqrt{2e|\Delta\Phi|/m_e}$ is the electron cut-off velocity (i.e., the parallel velocity of an electron reflected at the wall with $v_\| = 0_+$), and $H(v)$ is the step function. In setting $v_\|\big|_{\rm Max} = v_c$ for the reflected electrons, we have used the fact that in the presence of a constant magnetic field and a slowly varying electric field ($\rho_e \ll \lambda_{\rm D}$), $v_\perp$ is an adiabatic constant.

For later reference, we define the "shift energy" of the fast electrons as

$$E_f^{\rm shift} \equiv \tfrac{1}{2} m_e v_{f\|}^2, \tag{4}$$

so that the average energy of the fast electrons at the sheath entrance can be approximated as

$$\langle E_f^{\rm kin}\rangle \equiv E_f^{\rm shift} + \tfrac{3}{2}T_f. \tag{5}$$

In addition to these slow and fast electrons we also have the secondary ones, whose distribution function $f_s^0(v_\parallel, v_\perp)$ need not be specified except for the assumption that their initial velocities are much smaller than v_c. Then we can write

$$n_s^0 = F_{\rm sx}/v_c, \tag{6}$$

where $F_{\rm sx}$ is the secondary-electron flux. Assuming that secondary-electron emission due to slow-electron and ion impact is negligible,[29] this flux can be expressed in the form

$$F_{\rm sx} = -\gamma F_{\rm fx}, \tag{7}$$

where γ is the effective secondary-electron emission coefficient due to fast-electron impact.[30–31]

In all cases considered in this work, we have that at the sheath entrance both the fast- and secondary-electron densities are much smaller than the thermal-electron density:

$$n_f^0/n_{\rm sl}^0 \ll 1, \quad n_s^0/n_{\rm sl}^0 \ll 1, \tag{8}$$

so that we are justified in assuming that the normal component of the ion average velocity at the sheath entrance, $-u_{ix}^0$, satisfies the "classical" Bohm–Chodura condition,[32]

$$u_{ix}^0 \equiv |F_{ix}|/n_e^0 \geqslant c_s \sin\varphi = \sqrt{(\gamma_i T_i + T_{\rm sl})/m_i}\sin\varphi, \tag{9}$$

where $\gamma_i = 5/3$ is the ion adiabatic constant and c_s is the ion-sound velocity. Note that the Bohm–Chodura condition (9) need not necessarily be satisfied marginally, i.e., u_{ix}^0 can exceed the value $c_s \sin\varphi$.[1] By contrast, the Bohm criterion is always satisfied marginally, i.e., the normal component of the ion fluid velocity at the Debye-sheath entrance is always (approximately) equal to c_s. Note that condition (9) is the only assumption we make about the ion distribution at the sheath entrance.

At this point, a question about the stability of the model described may arise. The two fast-electron beams (incoming and reflected) included in our model can cause the plasma–beam instability.[33] Here we make the assumption that the instability is damped by collisions (or other mechanisms) in the collisional presheath and bulk plasmas, so that the oscillation amplitude does not exceed the linear level. Hence, we can consider time-independent quantities averaged over the oscillation period. We wish to note that the same assumption also has to be made for plasma sheaths without energetic electrons, because the secondary electrons released from the wall practically represent a monoenergetic beam which propagates into the plasma and can cause the same kind of instability as shown in Refs. 34 and 35 (which, however, is usually neglected).

Substituting the distribution functions (3) into the expression for the particle fluxes,

$$F_{kx} = 2\pi\sin\varphi \int_{-\infty}^{+\infty} dv_\parallel v_\parallel \int_0^\infty dv_\perp v_\perp f_s^0(v_\parallel, v_\perp) \quad (k = {\rm sl}, f);$$

Eq. (2) becomes

$$\left(n^0 u_{ix}^0 + \frac{J}{e}\right) \Big/ \sin\varphi$$
$$= n_{\rm sl}^0 v_{{\rm sl}T}[\sqrt{\pi}(1+\mathrm{erf}(v_c/v_{{\rm sl}T}))]^{-1}\exp(-v_c^2/v_{{\rm sl}T}^2)$$
$$+ n_f^0\left[\frac{1}{\sqrt{\pi}} v_{fT}\exp(-(v_c - v_{f\parallel})^2/v_{fT}^2) + v_{e\parallel}\right.$$
$$\left.\times\{1-\mathrm{erf}((v_c - v_{f\parallel})/v_{fT})\}\right](1-\gamma)[1+2\,\mathrm{erf}(v_{f\parallel}/v_{fT})$$
$$+ \mathrm{erf}((v_c - v_{f\parallel})/v_{fT})]^{-1}. \tag{10}$$

Then, introducing the dimensionless quantities,

$$n^* = n_f^0/n^0, \quad \alpha = \sqrt{T_{\rm sl}/T_f}, \quad \beta = v_{f\parallel}/v_{fT},$$
$$c = \sqrt{\pi}\frac{u_{ix}^0 + J/en^0}{v_{{\rm sl}T}\sin\varphi}, \quad \Delta\Psi = e|\Delta\Phi|/T_{\rm sl},$$

we obtain from Eq. (10),

$$n^* = \alpha\frac{[c - A(0,\sqrt{\Delta\Psi})][A(\beta, \alpha\sqrt{\Delta\Psi} - \beta) - \alpha A(0,\sqrt{\Delta\Psi})]^{-1}}{1 - \gamma(1 + A(0,\sqrt{\Delta\Psi})/\sqrt{\pi\Delta\Psi})}, \tag{11}$$

with

$$A(\eta, y) = \frac{\exp(-y^2) + \sqrt{\pi}\eta(1-\mathrm{erf}\, y)}{1 + 2\,\mathrm{erf}(\eta) + \mathrm{erf}\, y},$$

where we have used Eqs. (6) and (7) for the secondary-electron density.

Equation (11) can be simplified if the fast-electron density is sufficiently large, i.e., for

$$n^* \gtrsim n^*(\Delta\Psi = \Delta\Psi') \approx \frac{\alpha c}{(1-\gamma)A(\beta, \alpha\sqrt{\Delta\Psi'} - \beta)}, \tag{12}$$

where

$$\Delta\Psi' = \max\{\Delta\Psi_0 + 3; |\ln(1-\gamma)|; (\beta^2+1)/\alpha^2\}. \tag{13}$$

Then Eq. (11) reduces to

$$n^* = \frac{\alpha c}{(1-\gamma)A(\beta, \alpha\sqrt{\Delta\Psi} - \beta)}. \tag{14}$$

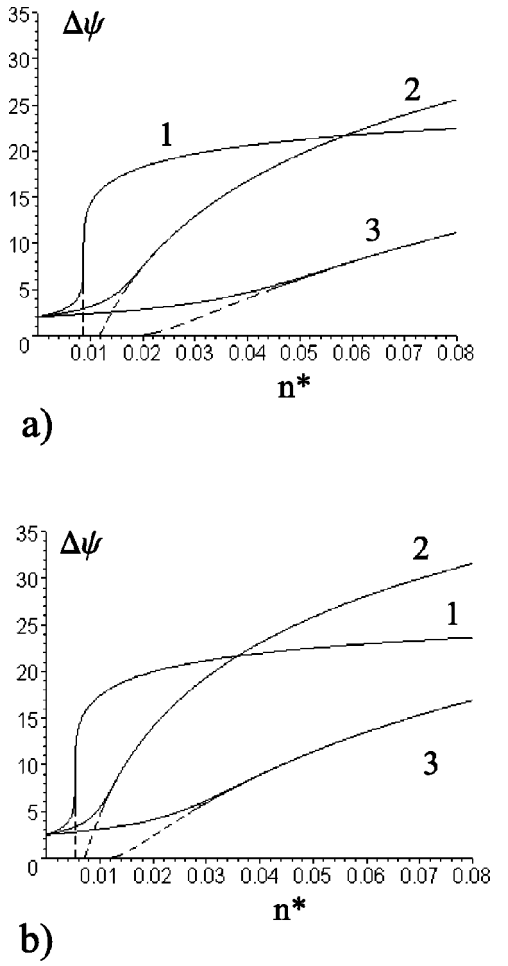

FIG. 2. Normalized floating potential ($J=0$) versus normalized fast-electron density for $u_{ix}^0=c_s \sin\varphi$ and $\gamma=0$, as obtained from the exact equation (11) (solid lines) and from the simplified equation (14) (dashed lines). (a) $T_i=T_{sl}$, (b) $T_i=0$. Curves 1, 2 and 3 correspond to $E_f^{shift}=57T_f=19T_{sl}$ (cold beam), $E_f^{shift}=3T_f/2=39T_{sl}/4$ (hot beam) and $E_f^{shift}=0$, $T_f=13T_{sl}$ (high-temperature electrons with zero shift velocity), respectively.

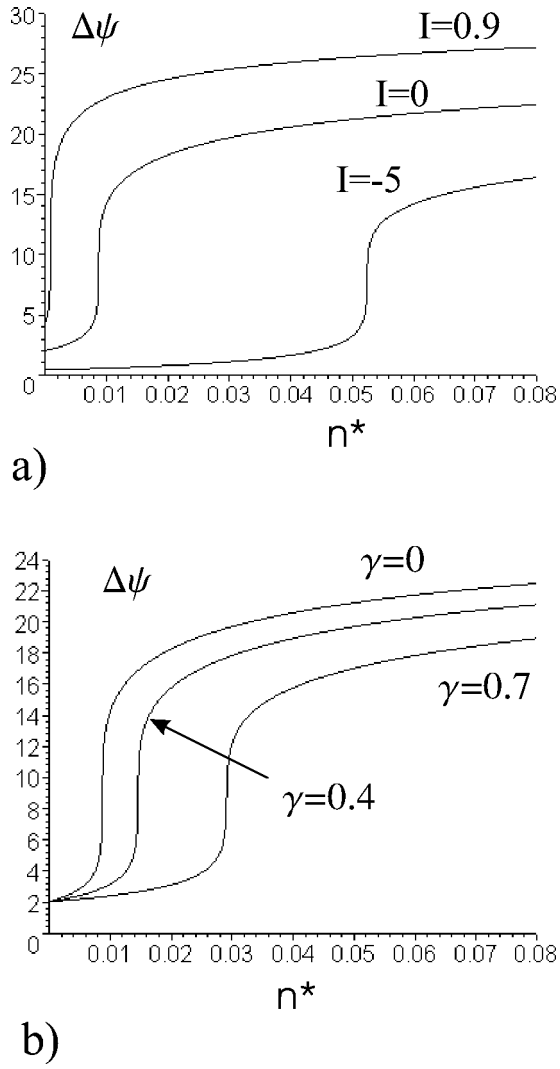

FIG. 3. Normalized potential drop across the sheath versus cold–fast-electron beam density for different regimes. In all cases, $u_{ix}^0=c_s \sin\varphi$, $T_i=T_{sl}=3T_f$, and $tE_f^{shift}=19T_{sl}$. (a) $\gamma=0$; (b) $I=0$.

Condition (12) ensures that the density n^* is above the region with steep gradients of the function $\Delta\Psi(n^*)$, where even a very small change of n^* can significantly influence $\Delta\Psi$ and the exact equation (11) has to be used.

B. Potential drop across the sheath

In Fig. 2 we show the normalized floating potential $\Delta\Psi(J=0)$ as a function of the normalized fast-electron density n^*, as obtained from Eqs. (11) (solid lines), and (14) (dashed lines). Curves for three different types of fast-electron population are plotted: (1) cold beam [$E_f^{shift}\gg T_f$, where E_f^{shift} is the shift energy defined in (4)], (2) a hot beam with the temperature comparable to the shift energy ($E_f^{shift}=3T_f/2$), and (3) high-temperature Maxwellian electrons with zero shift velocity ($E_f^{shift}=0$). Parameters are chosen such that far from the wall all types of fast electrons have the same average kinetic energy $\langle E_f^{kin}\rangle$ given by Eq. (5). Figures 2(a) and 2(b) correspond to the cases $T_i=T_{sl}$ and $T_i=0$, respectively.

In all cases we see that for realistic plasma parameters even a small population of fast electrons can significantly change the floating potential. For very small fast-electron densities, their influence is strongest for a cold beam, whereas with increasing fast-electron density their effect becomes strongest for a hot electron beam. Also note that in the case of the cold electron beam there exists a region where $\partial\Delta\Psi/\partial n^*\gg 1$ and the floating potential becomes very sensitive to the beam density.

For convenience, we introduce the quantity

$$I\equiv -J/en^0u_{ix}^0,$$

which we refer to as the ''normalized current to the wall,'' or simply as the ''current.'' The normalized potential drop $\Delta\Psi$ for different currents and different secondary-electron emission coefficients γ in the case of a cold fast-electron beam is given in Fig. 3. Analogous results are also obtained when the fast-electron population represents a hot beam or hot electrons with zero shift velocity. These plots show again that in all regimes the potential drop across the sheath is very sensitive to the presence of a fast-electron population.

It is instructive and important to know the critical value of n^* at which the fast electrons change significantly the potential drop across the sheath. To be specific, let us consider the value $n^*=n_c^p$ at which $\Delta\Psi$ doubles:

$$\Delta\Psi(n_c^p)=2\Delta\Psi_0, \tag{15}$$

where $\Delta\Psi_0$ is the potential drop in the absence of the fast-electron population:

$$\Delta\Psi_0\approx\ln\frac{1}{2c}. \tag{16}$$

Inserting expressions (15) and (16) into Eq. (11), we find

$$n_c^p=\alpha\frac{[c-A(0,\sqrt{2|\ln 2c|})][A(\beta,\alpha\sqrt{2|\ln 2c|}-\beta)-\alpha A(0,\sqrt{2|\ln 2c|})]^{-1}}{1-\gamma(1+A(0,\sqrt{2|\ln 2c|})/\sqrt{2\pi|\ln 2c|})}. \tag{17}$$

In Fig. 4, n_c^p is plotted as a function of the normalized fast-electron average kinetic energy,

$$\epsilon=\langle E_f^{\rm kin}\rangle/\langle E_{sl}^{\rm kin}\rangle=(2\beta^2/3+1)/\alpha^2,\quad \langle E_{sl}^{\rm kin}\rangle\equiv 3T_{\rm sl}/2.$$

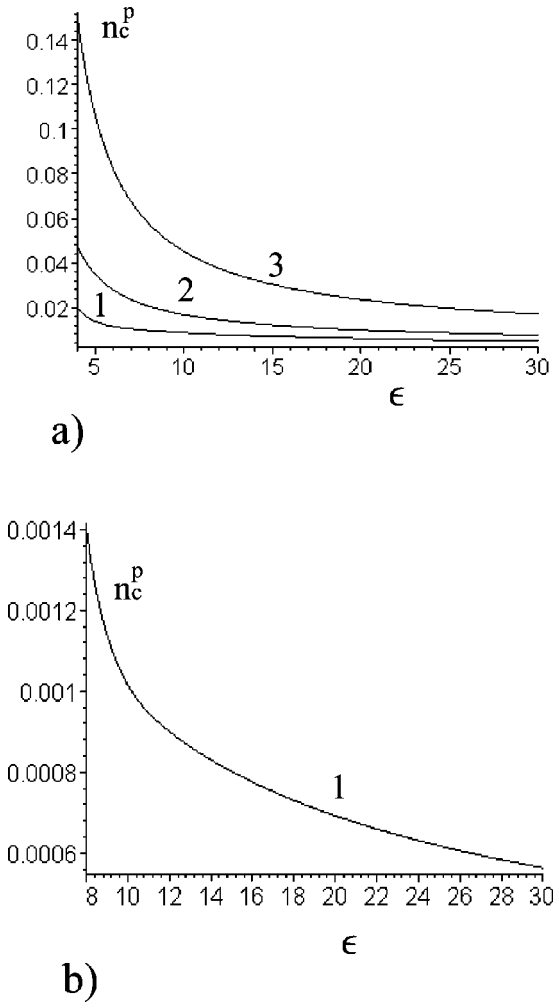

FIG. 4. Normalized critical density n_c^p as a function of the normalized fast-electron average energy ϵ for $u_{ix}^0=c_s\sin\varphi$, $T_i=T_{\rm sl}$ and $\gamma=0$. (a) $I=0$, (b) $I=0.9$. Curves 1, 2 and 3 correspond to $E_f^{\rm shift}=57T_f=19T_{\rm sl}$, $E_f^{\rm shift}=3T_f/2=39T_{\rm sl}/4$ and $E_f^{\rm shift}=0$, $T_f=13T_{\rm sl}$, respectively; cf. Fig. 2.

The critical density decreases with increasing current to the wall and with decreasing beam temperature (for fixed kinetic energy). From Fig. 4(b) we see that for reasonable plasma parameters n_c^p can be smaller than 10^{-3}.

C. Energy flux to the wall

In order to obtain the energy deposited at the wall ($\Theta_l^{\rm wall}>0, l=i,e$) we use the equation of energy conservation. Since, according to our assumptions, the plasma sheath is one-dimensional and collisionless, we have

$$\partial_x\Theta_{lx}=-e_lF_{lx}\partial_x\Phi(l=i,e),$$

where e_l is the particle charge and Θ_{lx} is the normal component of the particle energy flux. We integrate these equations to obtain

$$\Theta_l^{\rm wall}=-\Theta_{lx}(x=0)=|\Theta_{lx}^0|+e_lF_{lx}\Delta\Phi\quad(l=i,e), \tag{18}$$

where Θ_{lx}^0 is the normal component of the species-l particle energy flux at the sheath entrance. For the slow- and fast-electron energy fluxes we have

$$\Theta_{kx}^0=\pi m_e\sin\varphi\int_{-\infty}^{+\infty}d\upsilon_\parallel\upsilon_\parallel\int_0^\infty d\upsilon_\perp\upsilon_\perp(\upsilon_\parallel^2+\upsilon_\perp^2)f_k^0(\upsilon_\parallel\upsilon_\perp)\quad(k=sl,f). \tag{19}$$

After substitution of the distribution functions (3) in this expression, and using the last equation of the system (18), the total electron energy flux to the wall is obtained as

$$\Theta_e^{\rm wall}=\Theta_0\sin\varphi\left[2A(0,\sqrt{\Delta\Psi})+\frac{n^*}{\alpha^3}\chi(\alpha,\beta,\Delta\Psi)\right], \tag{20}$$

with

$$\chi(\alpha,\beta,\Delta\Psi)=A(\beta,\alpha\sqrt{\Delta\Psi}-\beta)[5/2+\beta^2-\alpha^2(\Delta\Psi+2\gamma A(0,\sqrt{\Delta\Psi})/\sqrt{\pi\Delta\Psi})]-2\alpha^3A(0,\sqrt{\Delta\Psi})+\exp[-(\alpha\sqrt{\Delta\Psi}-\beta)^2]\times\frac{\alpha^2\Delta\Psi+\alpha\beta\sqrt{\Delta\Psi}-1/2}{1+2\,\mathrm{erf}(\beta)+\mathrm{erf}(\alpha\sqrt{\Delta\Psi}-\beta)},$$

where

$$\Theta_0 = n^0 v_{slT} T_{sl}/\sqrt{\pi}$$

is the energy flux associated with the half-Maxwellian (thermal) electron distribution.

For the ions we have

$$\Theta_i^{wall} = |\Theta_{ix}^0| + n^0 u_{ix}^0 T_{sl} \Delta\Psi. \tag{21}$$

If the ion distribution at the sheath entrance is a cut-off Maxwellian,

$$f_i^0(v_\parallel, v_\perp) = 2n^0 \frac{\exp[-((v_\parallel^2 + v_{i\parallel})^2 + v_\perp^2)/v_{iT}^2] H(-v_\parallel)}{v_{iT}^3 \pi^{3/2}(1+\mathrm{erf}(v_{i\parallel}/v_{iT}))} \tag{22}$$

($v_{iT} = \sqrt{2T_i/m_i}$ and $-v_{i\parallel}$ are ion thermal and shift velocities, respectively), then

$$u_{ix}^0 = \sin\varphi \left[v_{i\parallel} + v_{iT} \frac{\exp(-v_{i\parallel}^2/v_{iT}^2)}{\sqrt{\pi}(1+\mathrm{erf}(v_{i\parallel}/v_{iT}))} \right] \tag{23}$$

and

$$\Theta_i^{wall} = n^0 v_{ix}^0 (m_i v_{i\parallel}^2/2 + 5/2 T_i + T_{sl}\Delta\Psi) - n^0 v_{iT} \sin\varphi (2T_i + v_{i\parallel}^2/2) \frac{\exp(-v_{i\parallel}^2/v_{iT}^2)}{\sqrt{\pi}(1+\mathrm{erf}(v_{i\parallel}/v_{iT}))}. \tag{24}$$

Using the Bohm–Chodura condition (9) in the marginal form we simplify Eqs. (23) and (24) to obtain the well-known expressions

$$v_{i\parallel} \approx c_s \tag{25}$$

and

$$\Theta_i^{wall} \approx n^0 c_s \sin\varphi [T_{sl}(1/2 + \Delta\Psi) + T_i(5+\gamma_i)/2]. \tag{26}$$

In Figs. 5 and 6 the energy flux to the wall is given versus the fast-electron density for different current regimes and different types of fast-electron populations. Like the potential drop across the sheath, the energy flux to the wall is, in all regimes, very sensitive to the density of any type of fast-electron population. For the high-temperature electron population with negligible fluid velocity, the electron component of the energy flux is dominant, except for the case with a large positive current flow towards the wall [$I>0$, Fig. 6(e)], when most electrons are reflected before they reach the latter. If the fast electrons have a non-negligible fluid velocity, the electron energy flux exhibits an interesting behavior. Initially it increases with n^*, but then becomes a decreasing function of n^* [see Figs. 5(a)–5(d) and 6(b)]. This effect becomes stronger with decreasing beam temperature, increasing secondary-electron emission coefficient, and increasing negative current to the wall ($I<0$). Moreover, for the cold electron beam it becomes so strong that even the total energy flux to the wall can decrease (!) with increasing beam density [Figs. 5(b) and 6(b)].

This ''strange'' behavior has the following explanation. For small n^* the potential drop in the sheath is sufficiently small and most of the fast electrons can still reach the wall, depositing their high energy there. With increasing n^*, more electrons reach the wall and the electron energy flux to the wall increases. However, at some critical n^* the potential drop becomes so large that all slow electrons are reflected before they reach the wall. With a further increase in n^*, the number of fast electrons reaching the wall per unit time does not change (since the current to the wall is fixed), but due to the increasing potential drop the kinetic energy carried by them decreases. An exception is the case of a high-temperature electron population with zero fluid velocity, when from some critical n_0^* on the electron energy flux does not change with the fast-electron density [Fig. 5(e)]. Figures 5(f), 6(d) and 6(f), with their monotonically increasing electron energy flux, correspond to densities smaller than n_0^*.

As already mentioned, the rate of impurity sputtering from the wall depends on the energy of the impinging ions. Hence, it is important to know the critical fast-electron density n_c^q at which the ion energy flux changes significantly, i.e., doubles:

$$\Theta_i^{wall}(n_c^q) = 2\Theta_i^{wall}(0).$$

For Maxwell-distributed ions (22) we find

$$n_c^q = \alpha \frac{[c - A(0, \sqrt{\Delta\Psi(n_c^q)})][A(\beta, \alpha\sqrt{\Delta\Psi(n_c^q)} - \beta) - \alpha A(0, \sqrt{\Delta\Psi(n_c^q)})]^{-1}}{1 - \gamma(1 + A(0, \sqrt{\Delta\Psi(n_c^q)})/\sqrt{\pi\Delta\Psi(n_c^q)})}, \tag{27}$$

where

$$\Delta\Psi(n_c^q) = 1/2 + 2\Delta\Psi_0 + 20T_i/6T_{sl} \approx 1/2 + 2|\ln 2c| + 20T_i/6T_{sl}. \tag{28}$$

For cold ions ($T_i \ll T_{sl}$) we have

$$n_c^q \approx n_c^p. \tag{29}$$

For hot ions ($T_i = T_{sl}$), the critical density n_c^q versus the fast-electron normalized energy ϵ is plotted in Fig. 7. These plots show that n_c^q (like n_c^p) decreases with increasing current to the wall and with decreasing fast-electron beam temperature. Figure 7(b) shows n_c^q for the most critical regime ($\gamma = 0, I \approx 1$). We see that for realistic plasma parameters n_c^q can be smaller than 10^{-3}.

III. SIMULATIONS

In order to check the analytical results obtained in the previous section, a number of computer simulations was per-

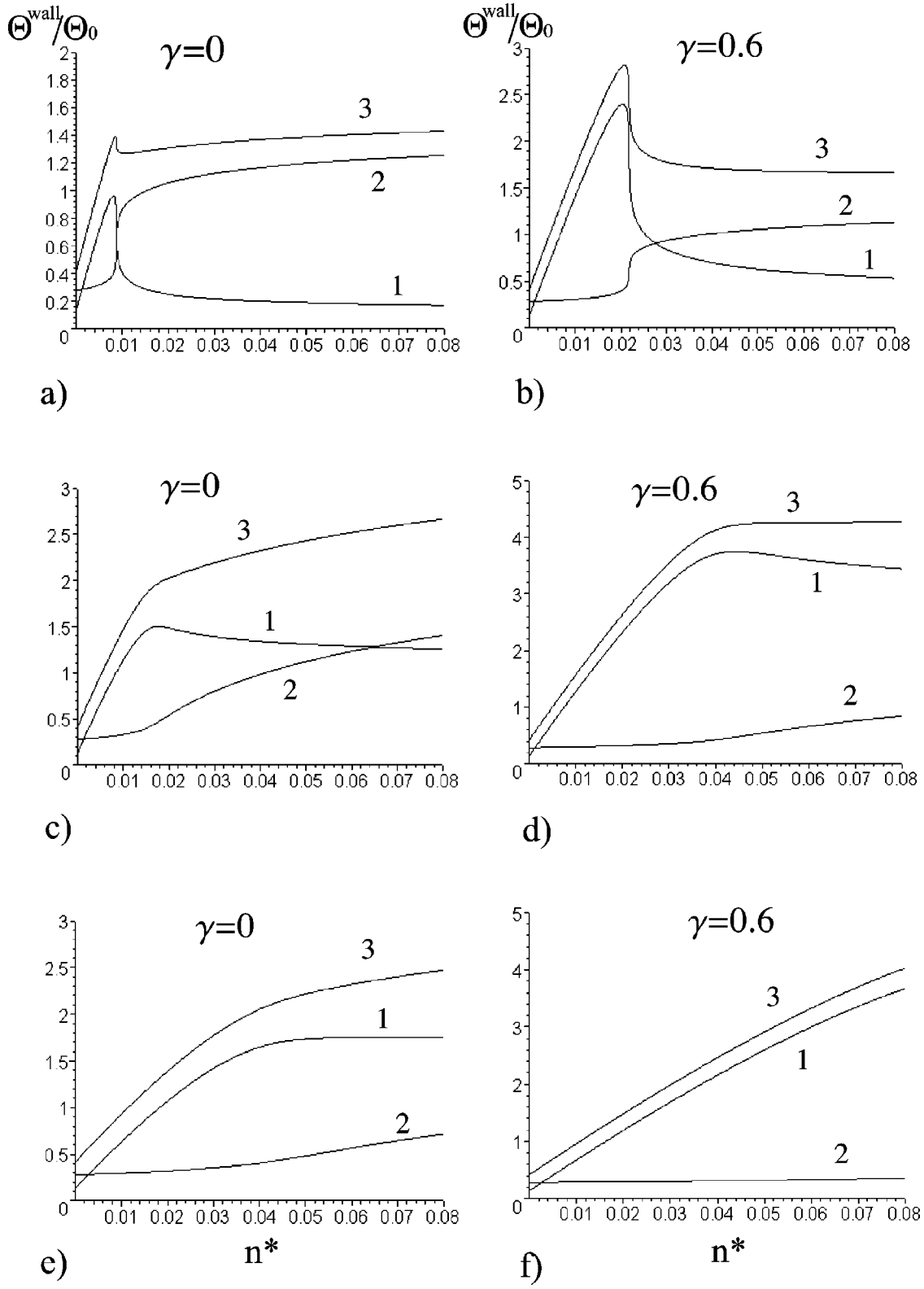

FIG. 5. Energy flux to the wall for the floating sheath ($I=0$). (a) and (b) for $E_f^{\text{shift}}=57T_f=19T_{\text{sl}}$ (cold fast-electron beam). (c) and (d) for $E_f^{\text{shift}}=3T_f/2=39T_{\text{sl}}/4$ (hot fast-electron beam). (e) and (f) for $E_f^{\text{shift}}=0$, $T_f=13T_{\text{sl}}$ (high-temperature electrons without shift velocity). At the sheath entrance, the ions are assumed to have the cut-off Maxwellian distribution (22), with $v_{i\|}=c_s$ and $T_i=T_{sl}$. Curves 1, 2 and 3 correspond to $\Theta_e^{\text{wall}}/\Theta_0$, $\Theta_i^{\text{wall}}/\Theta_0$ and $(\Theta_e^{\text{wall}}+\Theta_i^{\text{wall}})/\Theta_0$, respectively.

formed with the 1d3v (one spatial and three velocity dimensions) PIC code XPDP1[36] with some modifications.

The simulation domain is shown in Fig. 1. At $t=0$, we start injecting Maxwell-distributed plasma particles [cf. (3) and (22)] into the empty system. The particles are injected at the $x=L$ (''injection'' or ''sheath entrance'') plane, whereas the wall, whose surface coincides with the $x=0$ plane, is assumed to be perfectly absorbing. The secondary electrons

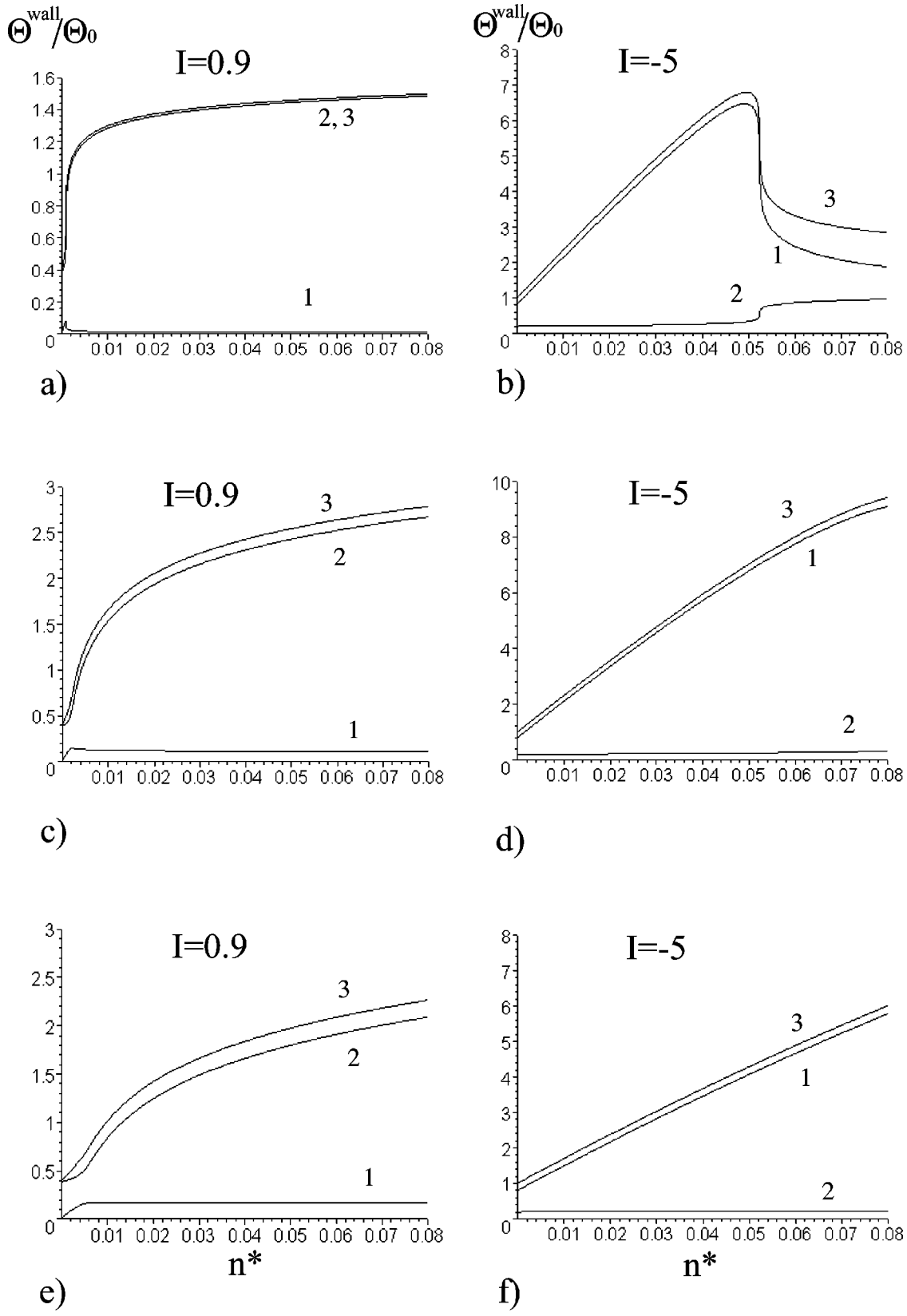

FIG. 6. Energy flux to the wall for different normalized current densities ($I=-J/en^0u_{ix}^0$). (a) and (b) for $E_f^{\text{shift}}=57T_f=19T_{\text{sl}}$ (cold beam). (c) and (d) for $E_f^{\text{shift}}=3T_f/2=39T_{\text{sl}}/4$ (hot beam). (e) and (f) for $E_f^{\text{shift}}=0$, $T_f=13T_{\text{sl}}$ (high-temperature electrons without shift velocity). At the sheath entrance, the ions are assumed to have the cut-off Maxwellian distribution (22), with $v_{i\|}=c_s$, and $T_i=T_{\text{sl}}$. Curves 1, 2 and 3 correspond to $\Theta_e^{\text{wall}}/\Theta_0$, $\Theta_i^{\text{wall}}/\Theta_0$ and $(\Theta_e^{\text{wall}}+\Theta_i^{\text{wall}})/\Theta_0$, respectively.

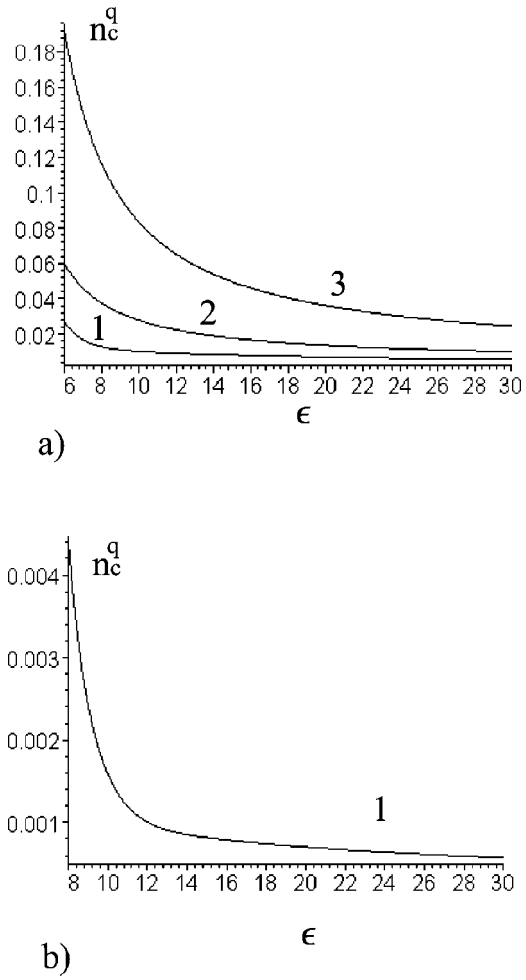

FIG. 7. Normalized critical density n_c^q as a function of normalized fast-electron average energy ϵ for $u_{ix}^0 = c_s \sin\varphi$, $T_i = T_{sl}$, $\gamma = 0$. (a) $I = 0$, (b) $I = 0.9$. Curves 1, 2 and 3 correspond to $E_f^{\text{shift}} = 57T_f = 19T_{sl}$, $E_f^{\text{shift}} = 3T_f/2 = 39T_{sl}/4$ and $E_f^{\text{shift}} = 0, T_f = 13T_{sl}$, respectively.

are injected from the wall with zero initial energy. The system reaches its stationary state after a few ion transit times, $t_{st} \approx (2-3)t_i$ $(t_i = L/v_{ix}^0)$. The injection parameters have been chosen so as to ensure quasi-neutral plasma at the entrance plane. High accuracy of the simulations is achieved by choosing a large number of superparticles per Debye length: 4000-8000 for thermal electrons and ions, and 60-600 for fast electrons. In these simulations, both the electron and ion motions are fully resolved.

For the plasma parameters we have chosen values relevant to contemporary LHCD experiments performed with the Tore Supra tokamak.[27] We have simulated the most critical case, i.e., when the fast-electron population represents a cold beam ($\beta = 7.45$). The simulation parameters are given in Table I.

We have simulated cases with different fast-electron densities, current regimes and secondary-electron emission coefficients. The main output of the simulations was the potential distribution in the sheath and the energy flux to the wall. These values were averaged over ten plasma oscillation periods. A typical potential distribution is plotted in Fig. 8, and the results obtained are summarized in Table II, where

TABLE I. Simulated plasma parameters.

Ion/electron mass ratio	$m_i/m_e = 1836$
Plasma density at sheath entrance	$n^0 = 1\times10^{18}$ m^{-3}
Ion temperature at sheath entrance	$T_i = 15$ eV
Slow-electron temperature	$T_{sl} = 30$ eV
Fast-electron temperature	$T_f = 10$ eV
Fast-electron shift velocity at sheath entrance	$v_{f\parallel} = 1{,}4\times10^7$ m/s ($\beta = 7.45$)
Magnetic field strength	$B = 3$ T
Magnetic-field inclination angle	$\varphi = 14°$
System length	$L = 0.2$ cm $= 50\lambda_D = 15\rho_i$
Number of grid cells	$N_x = 50$

the deviations indicate the (numerical and physical) fluctuations about the averaged values. For comparison we show the corresponding analytical results obtained from Eqs. (11), (20) and (26). In most cases, the difference between the analytical and simulation results is seen to be smaller than or equal to 4%. Exceptions are the electron energy flux for regimes with positive current to the wall ($I > 0$), and the potential drop for the floating case with "large" fast-electron density ($n^* = 0.05$) in the presence of secondary electrons.

The disagreement in the electron energy flux is easy to explain. In the regime with positive current to the wall (near the ion saturation current) only a small number of simulation electrons can reach the wall, so that the accuracy of the simulated electron energy flux is low. More difficult to explain are the large fluctuations observed in the floating case with "large" fast-electron density in the presence of secondary electrons. The fluctuation vanishes for the regime with positive current to the wall, or with decreasing secondary-electron emission. The high accuracy of the simulations and the good agreement of all other simulation results with the analytical ones indicate that these oscillations are not of a numerical nature. This type of oscillation, which can arise in the presence of three types of electrons in the sheath (thermal electrons, sufficiently dense high-energy electron beam, and secondary electrons), will be the subject of future work.

IV. CONCLUSIONS

The main results of our analytical calculations and PIC simulations can be summarized as follows.

For a given plasma density at the sheath entrance, the presence of even a small population of fast electrons can

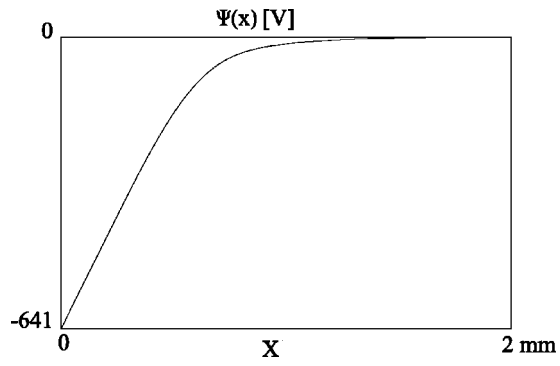

FIG. 8. Potential (V) averaged over ten plasma oscillation periods. The case with $\gamma = J = 0$, $n^* = 0.05$.

TABLE II. Obtained results.

			Theory			*Simulations*		
n^*	γ	I	$\Delta\Psi$	$\theta_e^{\text{wall}}\frac{\text{MW}}{\text{m}^2}$	$\theta_i^{\text{wall}}\frac{\text{MW}}{\text{m}^2}$	$\Delta\Psi$	$\theta_e^{\text{wall}}\frac{\text{MW}}{\text{m}^2}$	$\theta_i^{\text{wall}}\frac{\text{MW}}{\text{m}^2}$
0	0	0	2.38	0.20	0.48	2.47 ± 0.02	0.20 ± 0.01	0.52 ± 0.02
0.006	0	0	6.0	1.31	0.84	5.85 ± 0.01	1.37 ± 0.02	0.87 ± 0.02
0.006	0.2	0	3.87	1.56	0.63	3.98 ± 0.03	1.56 ± 0.02	0.68 ± 0.02
0.006	0.6	0	2.85	1.74	0.53	3.0 ± 0.3	1.77 ± 0.02	0.57 ± 0.02
0.05	0	0	21.7	0.26	2.39	21.4 ± 0.1	0.28 ± 0.02	2.5 ± 0.1
0.05	0.2	0	21.1	0.34	2.34	*Oscillations*	0.37 ± 0.02	2.5 ± 0.1
0.05	0.6	0	19.1	0.82	2.13	*Oscillations*	1.8 ± 0.7	2.2 ± 0.1
0.05	0	0.9	26.5	0.020	2.87	25.6 ± 0.1	0.035 ± 0.005	3.0 ± 0.1
0.05	0.2	0.9	26.1	0.025	2.83	25.1 ± 0.1	0.043 ± 0.001	2.93 ± 0.02
0.05	0.6	0.9	24.8	0.05	2.70	23.7 ± 0.1	0.09 ± 0.01	2.8 ± 0.1

significantly influence the potential drop across the sheath and the energy flux to the wall. For realistic plasma parameters ($\epsilon\equiv\langle E_f^{\text{kin}}\rangle/\langle E_{sl}^{\text{kin}}\rangle\gtrsim 10$), a fast-electron population with a relative density smaller then 0.1% (!) can double the potential drop across the sheath and the energy flux to the wall. The presence of a few percent of fast electrons can enhance these values by up to one order of magnitude.

When the fast-electron density exceeds a certain value, the electron energy flux to the wall exhibits an interesting behavior in that it decreases with increasing fast-electron density (for fixed other parameters). For a low-temperature fast-electron beam this effect is so strong that with increasing fast-electron density the total energy flux to the wall decreases as well.

The fast electrons become more influential with increasing current to the wall (decreasing J) and decreasing secondary-electron emission. For small fast-electron densities, their influence increases with decreasing temperature (for fixed energy). By contrast, the effect of the hot beam becomes stronger for larger densities.

The good agreement of analytical and simulation results shows that Eqs. (11), (14), (20) and (26) are accurate and can be used for different 1d plasma sheath models with two electron populations (assuming that at the sheath edge the distribution of each electron populations is well approximated by a cut-off Maxwellian). An exception is the case when in addition we have secondary electrons released from the wall. In this case, and if the current to the wall is small, a sufficiently large fast-electron density can cause high-amplitude oscillations in the plasma sheath.

The total potential drop between the wall and the ''unperturbed'' plasma far from the wall is the sum of the potential drops across the plasma sheath and the collisional plasma presheath. The maximum potential drop in an unmagnetized collisional plasma presheath cannot exceed a certain value $\Delta\Psi_{\max}$. Using different approaches, different results were obtained: $\Delta\Psi_{\max}=1.8$,[19] or $\Delta\Psi_{\max}=2.55$.[16] These values correspond to a large fast-electron population ($n^*\approx 0.3$), when there still exists a plasma sheath. We expect that this limit is valid also for the magnetized collisional plasma presheath. If fast electrons represent only a few percent (which is the case considered here) then the potential drop in the collisional presheath should be smaller then $\Delta\Psi_{\max}$, and in most cases, it will be negligibly smaller than the potential drop in the plasma sheath. Hence, in the presence of the fast-electron population the total potential drop between the wall and the ''unperturbed'' plasma can be approximated by the potential drop across the sheath.

Finally, let us note that the magnetized plasma sheath with a magnetic field perpendicular to the wall ($\varphi=\pi/2$) is equivalent to the unmagnetized one. Hence, all results obtained are also applicable to the unmagnetized plasma sheath.

ACKNOWLEDGMENTS

We thank the Plasma Theory and Simulation Group (head: Professor C. K. Birdsall) from the University of California at Berkeley, for providing us with the XPDP1 code, and Dr. M. Goniche, Dr. D. Guilhem, and Dr. J. Gunn from Tore Supra, C.E.A. Cadarache, France, for valuable discussions.

This work was supported by the Austrian Science Fund (FWF) Grants No. P12477-TPH and No. P15013, and performed within the Association Euratom-ÖAW. Its content is the sole responsibility of the authors and does not necessarily represent the view of the Commission or its Services. One of the authors (V.P.) acknowledges support from Czech GA CR Grant No. 202/00/1217.

[1] P. C. Stangeby, *The Plasma Boundary of Magnetic Fusion Devices* (Institute of Physics, Bristol, 2000), p. 98.
[2] E. R. Harrison and W. B. Thompson, Proc. Phys. Soc. London **74**, 145 (1959).
[3] R. Chodura, in *Physics of Plasma–Wall Interactions in Controlled Fusion* (Plenum, New York, 1986), p. 99.
[4] P. C. Stangeby, in Ref. 3, p. 41.
[5] K.-U. Rieman, J. Phys. D **24**, 493 (1991).
[6] P. C. Stangeby, Plasma Phys. Controlled Fusion **37**, 1031 (1995).
[7] K. Sato and F. Miyawaki, National Institute for Fusion Science, Report 136, 1992.
[8] R. W. Boswell, A. J. Lichtenberg, and D. Vender, IEEE Trans. Plasma Sci. **20**, 62 (1992).
[9] S. Mizoshita and K. Shiraishi, J. Nucl. Mater. **220–222**, 488 (1995).
[10] K. Shiraishi, N. Ohno, and S. Takamura, J. Plasma Fusion Res. **69**, 1371 (1993).
[11] S. B. Song, C. S. Chang, and D. Choi, Phys. Rev. E **55**, 1213 (1997).
[12] M. Čerček, T. Gyergyek, and M. Stanojevic, Contrib. Plasma Phys. **39**, 541 (1999).
[13] S. Meassick, M. H. Cho, and N. Hershkowitz, IEEE Trans. Plasma Sci. **13**, 115 (1985).

[14]L. Schot, Phys. Fluids **30**, 1795 (1987).
[15]S. G. Ingram and N. St. J. Braithwaite, J. Phys. D **23**, 1648 (1990).
[16]J. W. Bradley and H. Amemiya, J. Phys. Soc. Jpn. **63**, 3295 (1994).
[17]J. W. Bradley and H. Amemiya, Jpn. J. Appl. Phys. **33**, 3578 (1994).
[18]N. Jelić, M. Čerček, M. Stanojevic, and T. Gyergyek, J. Phys. D **27**, 2487 (1994).
[19]J. W. Bradley, J. Phys. D **29**, 706 (1996).
[20]R. Miyano, S. Izumi, R. Kitada, M. Fujii, S. Ikezawa, and A. Ito, Plasma Sources Sci. Technol. **6**, 551 (1997).
[21]R. H. Cohen and D. D. Ryutov, Phys. Plasmas **5**, 808 (1998).
[22]D. Tskhakaya, S. Kuhn, V. Petržilka, and R. Khanal, *Europhysics Conference Abstracts*, 26th EPS Conference on Controlled Fusion and Plasma Physics, Maastricht, 1999, edited by B. Schweer, G. Van Oost, and E. Vietzke (European Physical Society, Petit-Lancy, 1999), Vol. 23J, p. 537.
[23]V. Fuchs, M. Goniche, Y. Demers, P. Jacquet, and J. Mailloux, Phys. Plasmas **3**, 4023 (1996).
[24]M. Goniche, D. Guilhem, P. Bibet *et al.*, Nucl. Fusion **38**, 919 (1998).
[25]V. Petržilka, J. A. Tataronis, F. Califano *et al.*, *Proceedings of Invited Papers*, International Joint Varenna–Lausanne Fusion Theory Workshop, Varenna, Lago di Como, Italy, 31 August–4 September 1998, edited by J. W. Connor, E. Sindoni, and J. Vaclavik (Italian Physical Society, Bologna, 1998), p. 95.
[26]K. M. Rantamäki, T. J. H. Pättikangas, S. J. Karttunen, X. Litaudon, and D. Moreau, Phys. Plasmas **5**, 2553 (1998).
[27]P. Ghendrih and the Tora Supra Group, Plasma Phys. Controlled Fusion **12B**, 207 (1997).
[28]R. Chodura, *Europhysics Conference Abstracts*, 19th EPS Conference on Controlled Fusion and Plasma Physics, Innsbruck, 1992, edited by W. Freysinger, K. Lackner, R. Schrittwieser, and W. Lindinger (European Physical Society, Petit-Lancy, 1992), Vol. 16c, p. 871.
[29]R. A. Langley *et al.*, Nucl. Fusion, special issue on ''Data Compendium for Plasma–Surface Interactions'' (1984), p. 94.
[30]S. Mizoshita, K. Shiraishi, N. Ohno, and S. Takamura, J. Nucl. Mater. **220–222**, 488 (1995).
[31]D. Tskhakaya and S. Kuhn, *7th International Workshop on Plasma Edge Theory in Fusion Devices (PET 7)*, Tajimi, Japan, 4–6 October 1999, Contrib. Plasma Phys. **40**, 484 (2000).
[32]R. Chodura, Phys. Fluids **25**, 1628 (1982).
[33]A. B. Mikhailovskii, *Instabilities of a Homogeneous Plasma* (Consultants Bureau, New York, 1974), Vol. 1, p. 11.
[34]R. N. Franklin and W. E. Han, Plasma Phys. Controlled Fusion **30**, 771 (1988).
[35]D. Tskhakaya and S. Kuhn, *2000 International Congress on Plasma Physics* combined with the 42nd APS-DPP Meeting, Quebec City, 23–27 October 2000, Vol. I, pp. 89–92, Bull. Am. Phys. Soc. **45** (7), 334 (2000).
[36]J. P. Verboncoeur, M. V. Alves, V. Vahedi, and C. K. Birdsall, J. Comput. Phys. **104**, 321 (1993).